Comparative Study Between Two Navier-Stokes Algorithms for Transonic Airfoils

Miguel R. Visbal* and Joseph S. Shang†
Air Force Wright Aeronautical Laboratories, Wright-Patterson Air Force Base, Ohio

A critical examination of several aspects of the numerical simulation of high Reynolds number transonic airfoil flows is presented. Subcritical and supercritical flowfields about an aft-cambered airfoil were generated by solving the mass-averaged Navier-Stokes equations with turbulence incorporated through an algebraic eddy viscosity model. The governing equations were solved on curvilinear body-fitted grids utilizing two different algorithms, i.e., MacCormack's explicit and Beam-Warming implicit. The numerical uncertainties associated with different schemes, grid resolution, artificial viscosity, and far-field boundary placement were investigated and found to be of the same order of magnitude or less than the corresponding uncertainties in the available experimental data. Comparison of computed and experimental results showed good prediction of all the essential flow features. However, detailed comparison of velocity profiles pointed out deficiencies of the turbulence model downstream of the shock-wave boundary-layer interaction, in the airfoil cove and in the near wake. Thin-layer and Navier-Stokes computed results were found to be in excellent agreement with each other.

Nomenclature

c	= airfoil chord
C_D, C_L	= section drag and lift coefficients, respectively
C_P	= pressure coefficient, $2(p-p_\infty)/\rho_\infty U_\infty^2$
C_P^*	= critical pressure coefficient ($M=1$)
M_∞	= freestream Mach number
p	= static pressure
Re_c	= chord Reynolds number, $\rho_\infty U_\infty c/\mu_\infty$
T	= temperature
u,v	= Cartesian velocity components
U	= velocity $(u^2+v^2)^{1/2}$
x,y	= Cartesian coordinates parallel and normal to airfoil chord, respectively
Y	= distance normal to airfoil surface
α	= angle of attack
μ	= molecular dynamic viscosity
ξ,η	= transformed body-fitted coordinates
ρ	= density

I. Introduction

In recent years, the numerical simulation of high Reynolds number transonic flows over airfoils has been presented in numerous publications. A comprehensive review of the subject can be found, for example, in Refs. 1 and 2 and therefore is not repeated here. This earlier work clearly illustrates the potential of Navier-Stokes numerical methods for evolving into a reliable predictive design technique. However, for this goal to be attained, two major problem areas still require further investigation. First, an assessment of the accuracy of the computed solutions must be conducted in order to clarify the uncertainties due to grid resolution, boundary condition formulation, and numerical damping. Second, a suitable turbulence model must be developed, capable of accurately describing flows containing transition, separation, wakes, and shock-wave/boundary-layer interactions. This second problem area clearly constitutes the pacing item in computational aerodynamics and will probably require a continued process of numerical evaluation of different turbulence modeling formulations. For this evaluation process to be meaningful, the degree of uncertainty associated with the numerical simulations must be established.

Since "exact" solutions are not generally available for complex transonic flows of interest, grid refinement studies constitute the only suitable alternative for accuracy assessment. Even for two-dimensional flows, this approach can be very costly in terms of computer resources, and therefore the accuracy of the numerical solutions is customarily judged by comparison with available experimental data. However, comparing computed and experimental results can be inconclusive due to 1) lack of numerical resolution, 2) uncertainties in the measurements (e.g., wind tunnel and probe interference), and 3) inability to isolate numerical errors from those due to turbulence modeling. With the advent of powerful computers, more detailed calculations of two-dimensional transonic viscous flows are now possible[3] and should help clarify some of the uncertainties inherent in the numerical simulations.

With the above background as motivation, the present research critically examines several aspects of the numerical solution of the Navier-Stokes equations for high Reynolds number transonic airfoil flows. This problem embodies many interesting flow features, such as leading- and trailing-edge regions, wake, and shock-wave/boundary-layer interactions. The particular configuration considered was a modified Whitcomb supercritical airfoil, denoted as DSMA 523.[4] This airfoil exhibits significant rear loading and a strong viscous/inviscid interaction as compared with more conventional sections having little or no aft camber. In addition, this airfoil was selected as one of the test cases for the 1980 Stanford Conference on Complex Turbulent Flows.[5]

Computations were performed using the mass-averaged Navier-Stokes equations[6] expressed in terms of general curvilinear coordinates and with turbulence represented by an algebraic eddy viscosity model.[7] The governing equations were solved in nearly orthogonal body-fitted grids[8] employing MacCormack's explicit scheme[9] and the implicit Beam-Warming algorithm.[10] These two most commonly used numerical schemes were chosen for their intrinsic differences in solving the system of governing equations. A direct comparison between the two algorithms was performed under

Received Dec. 22, 1984; presented as AIAA Paper 85-0480 at the AIAA 23rd Aerospace Sciences Meeting, Reno, NV, Jan. 14-17, 1985; revision received May 1985.

*Visiting Scientist. Member AIAA.
†Technical Manager. Associate Fellow AIAA.

identical mesh systems, boundary conditions, and turbulence model. Such a one-to-one comparison, the authors believe, has not been previously documented in the literature.

The main objectives in this investigation of transonic airfoil flows can be summarized as follows:

1) A comparative study of the relative accuracy of an explicit vs implicit Navier-Stokes code.

2) Effects of grid refinement, numerical damping, and far-field boundary placement on the computed flowfields.

3) Comparison of the results obtained with the Euler, the thin-layer, and the full Navier-Stokes equations.

4) Evaluation of the algebraic turbulent eddy viscosity model by detailed comparison of computed and experimental data for both sub- and supercritical flows.

II. Governing Equations

The governing equations are taken to be the two-dimensional compressible Navier-Stokes equations expressed in terms of mass-averaged variables[6] and general curvilinear coordinates. Two different forms of the equations are employed in this research. The explicit numerical algorithm utilizes the chain-rule conservative form,[11] while the implicit scheme solves the strong conservative formulation.[12] The fluid is assumed thermally and calorically perfect. The molecular dynamic viscosity μ is given by Sutherland's law, and a constant molecular Prandtl number ($Pr=0.72$) is employed. Turbulence is simulated by a modified version of the algebraic eddy viscosity model of Baldwin and Lomax.[7] A detailed description of the turbulence model can be found in Refs. 13 and 14.

In order to define the problem completely, suitable boundary and initial conditions must be specified. Referring to the airfoil computational domain shown in Fig. 1, the following boundary conditions are prescribed. Along the outer boundary ABC, freestream conditions are given for all the flow variables. On the downstream boundaries CD and AE, the pressure is set equal to its freestream value, and extrapolation is used for ρ, u, and v. Along the airfoil surface, the no-slip adiabatic conditions

$$u=v=0, \quad \frac{\partial}{\partial \eta}\left[\frac{p}{T}\right]=0 \tag{1}$$

are imposed. Finally, at the wake cut, averaging is used for all the flow variables in order to ensure continuity.

Since only steady flows are considered in this research, initial conditions are not of primary concern to provide a converged numerical solution. A uniform flow initial condition was employed in the present airfoil calculations, unless previous computed results were already available.

III. Numerical Procedure

Body-fitted finite difference grids were generated about the airfoil using the method of Visbal and Knight.[8] A typical C-grid, shown in Fig. 1, is nearly orthogonal and displays substantial clustering in the viscous regions and in the airfoil leading- and trailing-edge areas.

Two separate Navier-Stokes solvers, namely, an explicit and an implicit code, were employed in the numerical solution of the flow equations. The implicit code solved the strong conservative form of the Navier-Stokes equations using the approximate-factored algorithm of Beam and Warming.[10] Euler time-differencing and second-order central spatial differences were utilized. Fourth-order explicit[12] and second-order implicit[15] damping terms were added to maintain stability. In order to accelerate convergence to steady state, a local time step[16] was employed. A similar version of the present implicit code had been previously validated for a variety of flow configurations.[17]

The explicit Navier-Stokes code solved the chain-rule form of the governing equations utilizing the unsplit predictor-corrector scheme of MacCormack.[9] As part of this algorithm, a fourth-order pressure damping term[18] was incorporated to control numerical oscillations. In order to improve the efficiency of steady flow computations, a local time step was introduced in the basic MacCormack's scheme. This was accomplished by specifying a constant Courant number throughout the computational domain.[14] The Courant number was typically assigned a value of 0.9. Unlike the implicit code, which was written for a scalar computer, the explicit solver is fully vectorized and exploits the vector-processing capabilities of the CRAY computer. Previous versions of this explicit Navier-Stokes code have been successfully applied to a variety of fluid dynamic problems.[2,19]

Since steady flowfields were obtained by time integration of the Navier-Stokes equations from a given initial condition, a suitable convergence criterion must be specified. Convergence was assessed by carefully monitoring the airfoil lift (C_L) and drag (C_D) coefficients. For all cases computed, the monitored coefficients approached a steady asymptote in a damped oscillatory fashion. Here, the flow was assumed converged when 1) the amplitude in the oscillations of C_L was less than 0.05-0.1% and 2) when the variations in C_D were within 1-2 drag counts (1 drag count = 0.0001). For the implicit algorithm, the corresponding root-mean-square value of the residual was typically 10^{-7} for all equations. Although, a more stringent convergence criterion could be stipulated, the present one was found to be suitable for engineering calculations.

IV. Results and Discussion

Computations were performed for an 11%-thick supercritical airfoil designated as DSMA 523.[4] This modified Whitcomb airfoil exhibits significant rear loading and strong viscous/inviscid interactions as compared to more conventional sections having little or no aft camber. The experimental data base[4] contains surface pressure distribution and velocity and density profiles along the upper surface, lower surface, and wake for a range of Mach number, Reynolds number, and angle of attack. Two specific cases were considered in this investigation, and the corresponding flow parameters are given in detail in Table 1.

Three different computational grids were employed in the present study. Details for these grids, which are referred to subsequently as coarse (92×31), medium (140×45), and fine (204×55), can be found in Table 2. The fine grid is shown in Fig. 1. A total of 23 different calculations were performed for the selected airfoil configuration using a CYBER 175 and

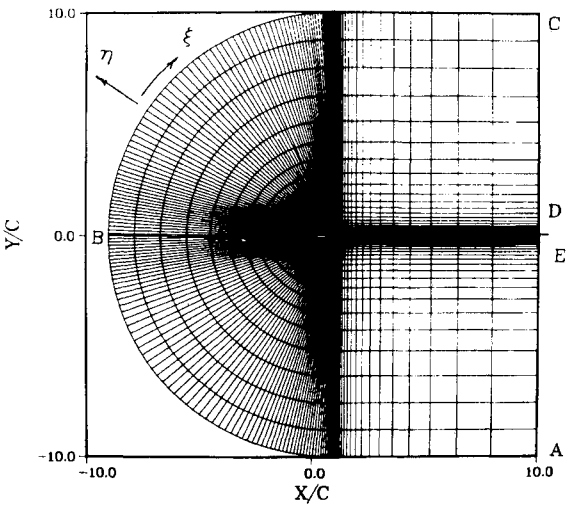

Fig. 1 Boundary-fitted grid.

Table 1 Flow parameters

Case	M_∞	Re_c	α, deg	x/c transition Upper	x/c transition Lower	Experimental C_L	Experimental C_D
Subcritical	0.6	4×10^6	2.6	0.05	0.18	0.58	0.011
Supercritical	0.8	2×10^6	1.8	0.35	0.18	0.65	0.017

Table 2 Grid details

Grid	IL × JL	$\Delta S_\xi/c$ min.	$\Delta S_\xi/c$ max.	$\Delta S_\eta/c$ min.	$\Delta S_\eta/c$ max.	No. of points on airfoil	ΔS_2^+ $M_\infty=0.6$	ΔS_2^+ $M_\infty=0.8$
Coarse	92×31	0.010	0.060	0.00025	1.03	58	18.5	—
Medium	140×45	0.005	0.050	0.00010	1.38	86	11.5	—
Fine	204×55	0.003	0.025	0.00005	1.25	150	6.9	2.1

NB.: IL, JL = No. of grid points in ξ and η directions, respectively; $\Delta S_\xi/c$ = Streamwise grid spacing on airfoil; $\Delta S_\eta/c$ = Grid spacing normal to airfoil surface; ΔS_2^+ = Normal spacing at airfoil surface in terms of law of the wall coordinates (upper surface, $x/c=0.5$).

the NASA Ames CRAY XMP computer. Only the most significant results are presented below for the subcritical and supercritical cases separately. More extensive results can be found in Ref. 14.

Results for Subcritical Case

Since in the experiments[4] the ratio of wind tunnel height to model chord was only four, interference effects are expected to be significant and must be accounted for (assuming the data are correctable) by adjustments in the freestream Mach number and angle of attack. Although the main objective of the present study is the comparison of the two numerical schemes, an attempt was made to determine the effective angle of attack for the subcritical case in order to provide a more meaningful comparison with the experiments. For this purpose, several computations were performed[14] with the implicit code on the coarse grid at various angles of attack. An angle of attack (α) of approximately 1.7 deg was required in order to match the experimental lift coefficient. All subsequent calculations were therefore performed with this value of α.

According to a formal truncation error analysis, the numerical smoothing terms are of high order and therefore their effects on the accuracy of the numerical solution are seldom considered. In the present study, the effects of artificial viscosity on the computed viscous flowfield were investigated on a limited basis. Calculations were carried out on the coarse mesh using both codes and different damping coefficients. For both schemes, the lift coefficients remained essentially unchanged with damping coefficient while C_D varied by as much as 30 drag counts. Since the effects of damping are expected to diminish as the mesh resolution increases, computations were performed on the fine grid using MacCormack's algorithm with two different damping coefficients differing by a factor of three. The corresponding variations in C_L and C_D with the damping coefficient were 0.3% and eight counts, respectively.

In order to investigate the effects of numerical resolution, the flowfield was computed on all three grid systems (Table 2) using both Navier-Stokes codes. The results for the explicit algorithm are displayed in Fig. 2. The computed lift coefficient increased monotonically with increasing resolution unlike the drag coefficient, which did not show any specific trend. The variations in C_L and C_D through the second mesh refinement were only 1% and 15 drag counts, respectively, as compared to 12% and 34 counts for the first grid refinement. Although some measure of numerical convergence is observed, the C_P distributions (Fig. 2) indicate that further resolution on the upper surface leading-edge area is still required. In addition, as the grid is refined, an embedded supersonic region (terminated by a shock) appears

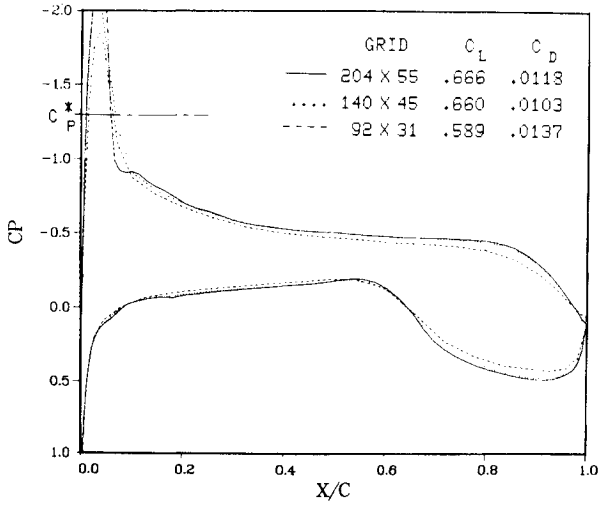

Fig. 2 Effect of grid resolution on computed subcritical flow, explicit algorithm.

near the airfoil leading edge.[13,14] The corresponding mesh refinement results for the implicit scheme displayed[13,14] a behavior similar to that of the explicit algorithm. For the implicit code, the variations in C_L and C_D after the second grid refinement were 2.2% and 5 drag counts, respectively.

A comparison between MacCormack and Beam-Warming results, as well as between the computed results and the experiment, is presented in Figs. 3 and 4 for the coarse and fine grids, respectively. The agreement between the two calculated C_P distributions improves as the mesh is refined. However, differences still persist on the airfoil upper surface immediately downstream of the embedded supersonic region. The computed lift and drag coefficients obtained with the two algorithms on the fine grid (Fig. 4) differ by 1.8% and 5 drag counts, respectively. These discrepancies are acceptable for engineering applications. The better agreement in C_L and C_D between the two numerical schemes on the coarse mesh (Fig. 3) can only be regarded as fortuitous.

In order to illustrate the importance of viscous effects for supercritical airfoils, the inviscid flowfield was computed with the implicit code on the coarse grid (Fig. 3). Even for a small angle of attack, subcritical flow without significant boundary-layer separation, the decrease in C_L due to viscous effects is substantial.

Referring to Fig. 4, the discrepancies in C_P and C_L between the fine-grid computational results and the experiments are in part due to uncertainties in the effective

freestream Mach number and angle of attack. The better prediction of the experimental lift coefficient on the coarse mesh (Fig. 3) simply points out that comparison with experimental data can be misleading unless proper numerical resolution criteria are first established.

A detailed comparison of computed and experimental velocity profiles is given in Figs. 5-7 for the airfoil upper surface, lower surface, and wake. As expected, the numerical profiles obtained with the explicit and implicit codes are in very good agreement with each other at all locations. On the suction surface (Fig. 5), the predicted profiles show higher values for the freestream velocity. This is consistent with the higher computed C_L (Fig. 4) and can be attributed mainly to uncertainties in the effective angle of attack. The discrepancies between the measured and computed velocity profiles at the airfoil cove (Fig. 6) and in the near wake (Fig. 7) are most likely due to deficiencies in the algebraic turbulent eddy viscosity model employed.

A qualitative comparison of computed density contours and an experimental interferogram is presented in Fig. 8. All typical features of the subcritical flow about the airfoil are discernible and in good qualitative agreement with the experimental flowfield.

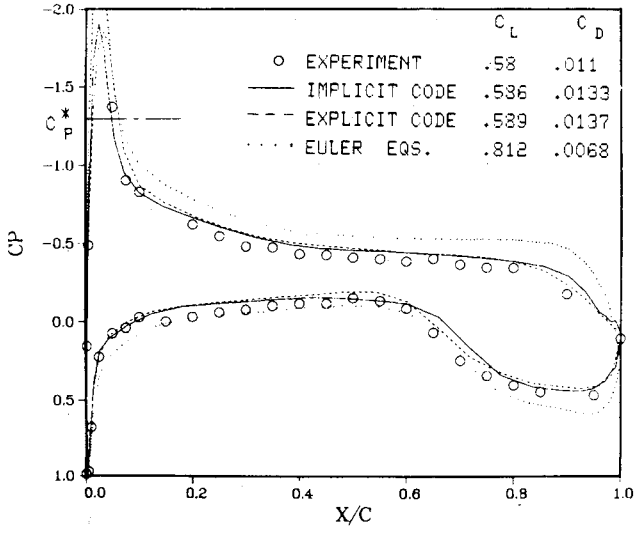

Fig. 3 Computed and experimental C_P, C_L, and C_D for subcritical case, coarse grid.

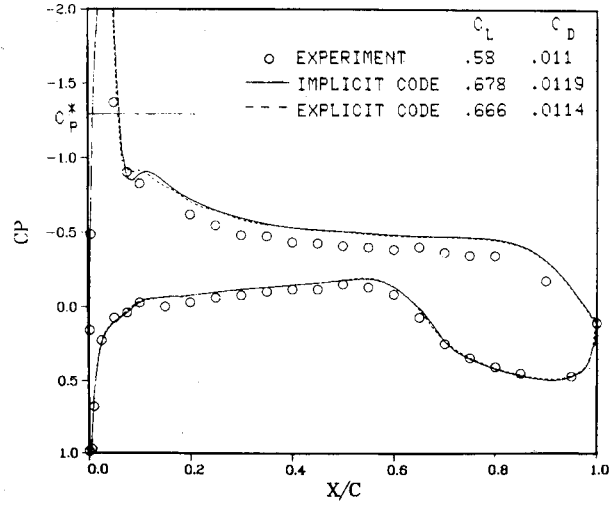

Fig. 4 Computed and experimental C_P, C_L, and C_D for subcritical case, fine grid.

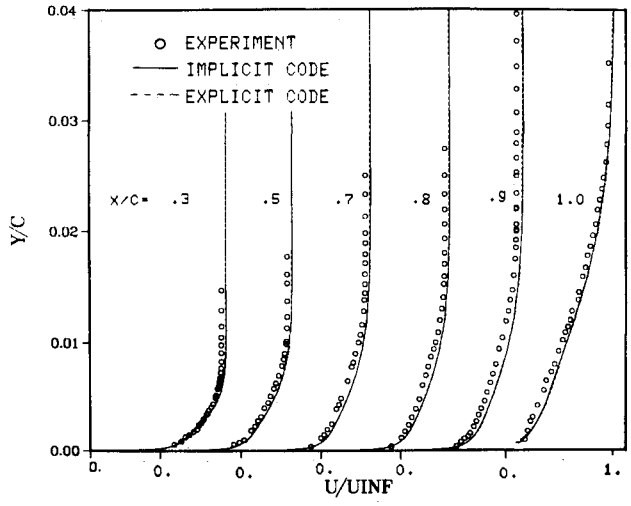

Fig. 5 Computed and experimental velocity profiles for subcritical case, upper surface.

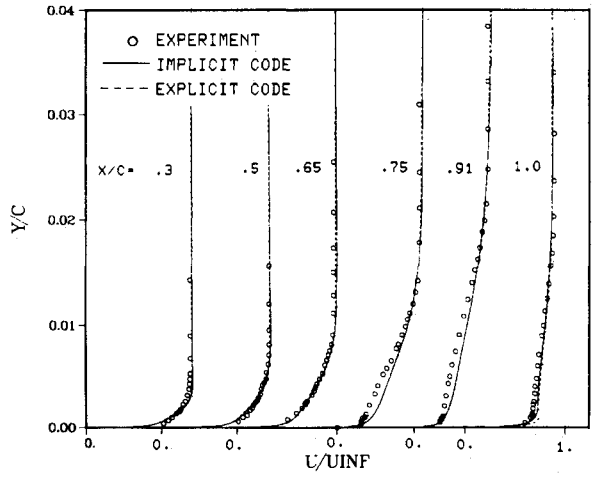

Fig. 6 Computed and experimental velocity profiles for subcritical case, lower surface.

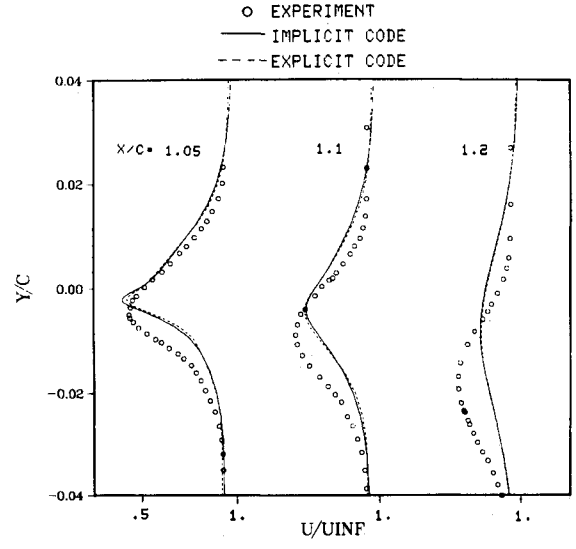

Fig. 7 Computed and experimental velocity profiles for subcritical case, near wake.

Results for Supercritical Case

Calculations for the supercritical flow case (Table 1) using both numerical algorithms were limited to the fine grid (Table 2). The coarser grid systems are not expected to provide sufficient spatial resolution.

In order to achieve a more meaningful comparison between computations and experiments, an attempt was made to determine the effective freestream Mach number and angle of attack. Computations at the nominal conditions ($M_\infty = 0.8$, $\alpha = 1.8$ deg) predicted[14] a shock location much further aft as compared to the experimental data. The freestream Mach number $M_\infty = 0.765$ and angle of attack $\alpha = 0.7$ deg were found to approximate the experimental shock position. These values were therefore employed in all subsequent calculations. As suggested in Ref. 5, the experimental C_P and C_L were corrected to account for the shift in Mach number by keeping a constant static-to-total pressure ratio. The present computations indicated that this supercritical airfoil is extremely sensitive to small variations in the freestream Mach number.

Since the far-field boundary conditions employed in this study are only approximate, the effect of the outer boundary placement on the numerical solution must be investigated. For this purpose, the supercritical flowfield was computed with the explicit algorithm for three different locations of the far-field boundary (namely, 10, 25, 50 chords away). The results for C_P, C_L, and C_D are shown in Fig. 9 and indicate that as the outer boundary is placed further away from the airfoil, the shock moves downstream with a corresponding increase in lift. This seems consistent with wall influence on airfoils. The difference in C_L between the 25- chord and 50-chord solution is only 1.8%. Although additional outward boundary placements have not been considered, it may be concluded that a computational domain extending at least 50 chords away from the airfoil should be employed for strong inviscid/viscous interacting calculations. The far-field boundary effects might be less significant for more conventional airfoils or for improved formulations of the boundary conditions.

A comparison of the computed results and experiments is presented below. Figure 10 displays reasonable agreement between the two numerical C_P distributions, except in the vicinity of the shock where additional spatial resolution in the streamwise direction is still needed. Both computed solutions fail to predict the measured static pressure on the upper surface downstream of the shock and on the lower surface cove. It appears that these discrepancies point out deficiencies in the algebraic turbulence model. A comparison of the velocity profiles on the upper surface, lower surface, and wake is given in Figs. 11, 12, and 13, respectively. The computed velocities are, as expected, in close agreement with each other. Discrepancies between the experimental and computed velocity profiles in the cove and near wake are apparent. Finally, a qualitative comparison of the experimental and numerical flowfields is presented in Fig. 14 in terms of computed density contours and the experimental interferogram.

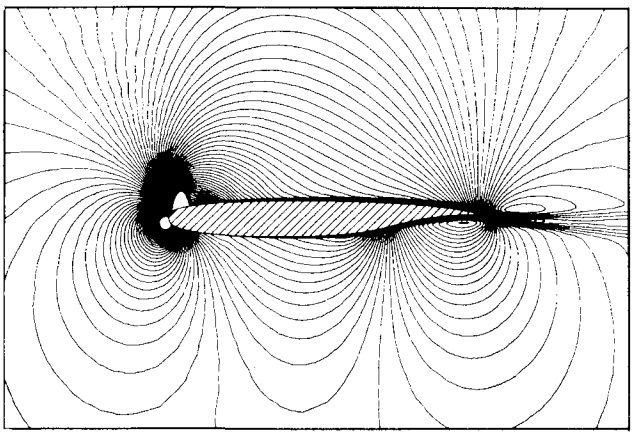

a) Explicit algorithm.

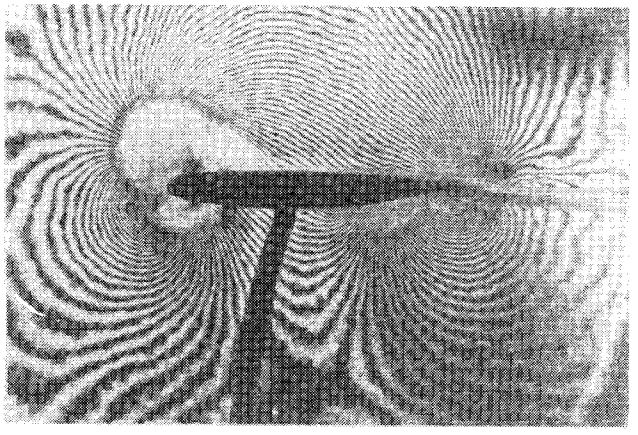

b) Experiment.

Fig. 8 Comparison of computed density contours and experimental interferogram, subcritical case.

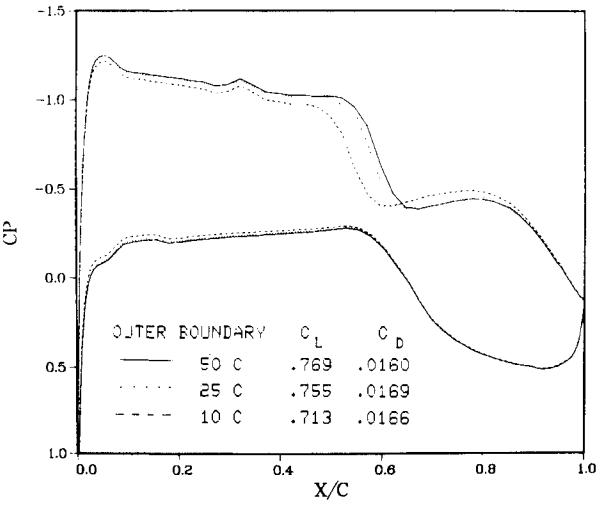

Fig. 9 Effect of far-field boundary placement on computed supercritical flow, explicit algorithm.

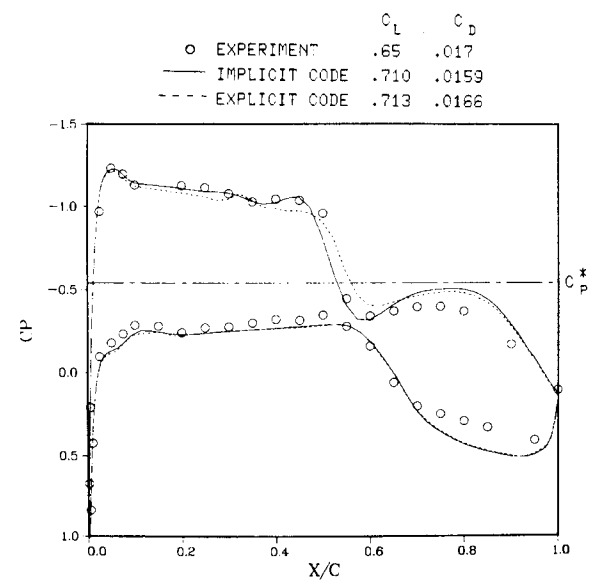

Fig. 10 Computed and experimental C_P, C_L, and C_D for supercritical case.

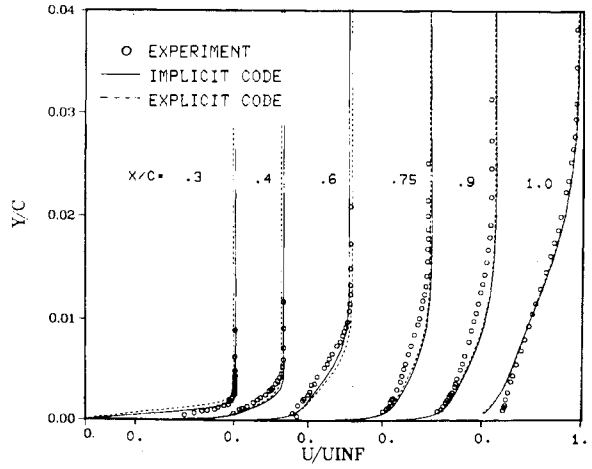

Fig. 11 Computed and experimental velocity profiles for supercritical case, upper surface.

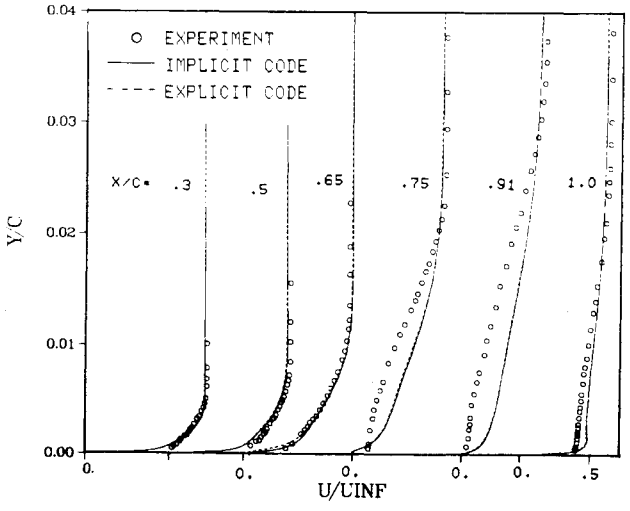

Fig. 12 Computed and experimental velocity profiles for supercritical case, lower surface.

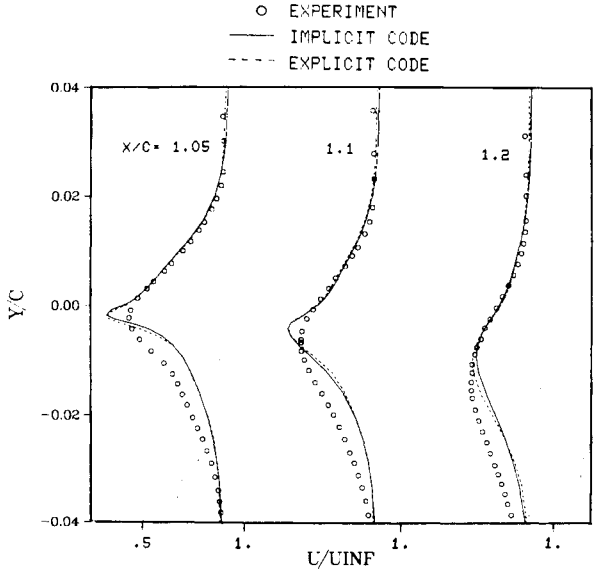

Fig. 13 Computed and experimental velocity profiles for supercritical case, near wake.

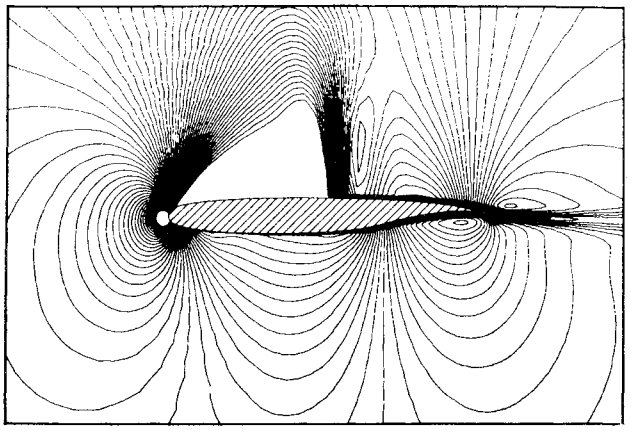

a) Implicit algorithm.

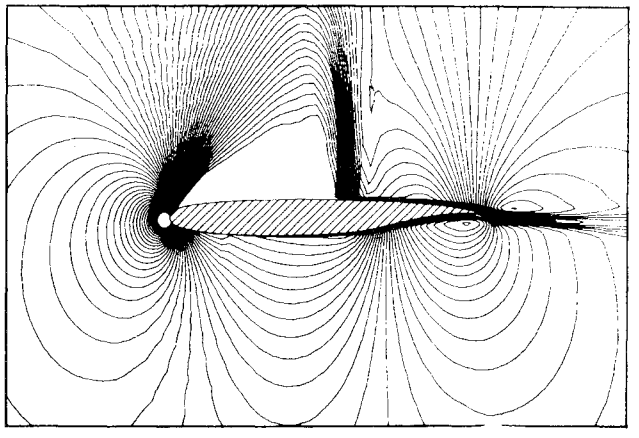

b) Explicit algorithm.

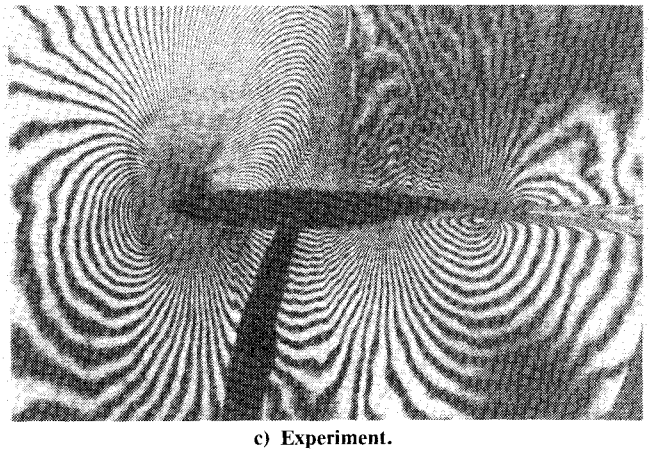

c) Experiment.

Fig. 14 Comparison of computed density contours and experimental interferogram, supercritical case.

It is interesting to compare the uncertainties in the numerical results of different algorithms with the repeatability in the experimental measurements. Figure 15, reprinted from Ref. 4, shows the pressure distributions obtained for the same nominal conditions during different wind tunnel runs. For this case, the experimental uncertainty is found to be of the same order of magnitude as that encountered in the numerical simulation (Fig. 10).

The thin-layer approximation has been commonly employed in the numerical solution of high Reynolds number airfoil flows,[20] and justification for its use can be found in Ref. 7. For unsteady transonic airfoils, significant discrepancies between the thin-layer and the full Navier-Stokes results were observed by Chyu and Kuwahara.[21] On the other hand,

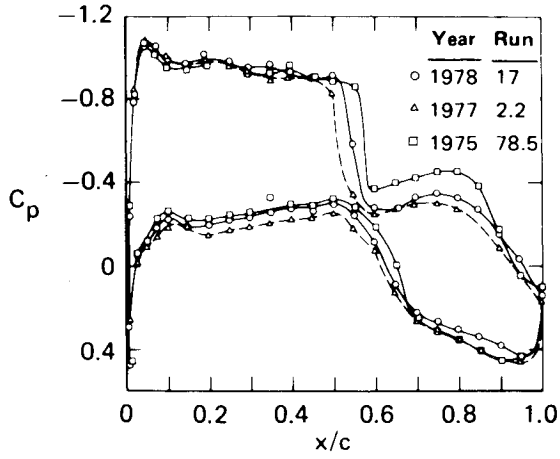

Fig. 15 Repeatability of experimental static pressure measurements for supercritical case (Ref. 4).

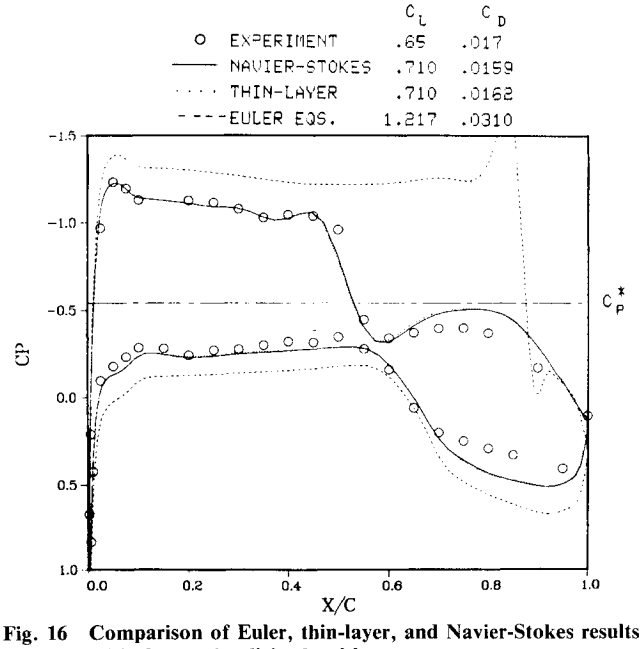

Fig. 16 Comparison of Euler, thin-layer, and Navier-Stokes results for supercritical case, implicit algorithm.

Degani and Steger[22] found good agreement between the two formulations when applied to a supersonic compression ramp. In the present study, the effect of the thin-layer approximation was investigated for the airfoil supercritical flow. The results, shown in Fig. 16, indicated very good agreement between the thin-layer and the full Navier-Stokes solution. Therefore, the use of the thin-layer equations is fully justified for this particular type of flow.

To illustrate the extent of the viscous/inviscid interaction effects for aft-cambered airfoils, the flowfield was also computed using the Euler equations. As Fig. 16 shows, the presence of the boundary layer modifies the flowfield dramatically. Viscous effects result in a much weaker shock (displaced upstream) and in a substantial decrease in the "plateau" loading. This is a direct consequence of boundary-layer displacement effects, which reduce the effective airfoil aft camber. The viscous lift coefficient is almost half the corresponding inviscid value.

Investigation of Numerical Error Due to Damping

An additional assessment of the accuracy of the computed solutions was performed by evaluating the amount of numerical damping relative to the truncation error and by comparing the physical and artificial viscosities. For the computed flowfield not to be seriously degraded by damping, the added smoothing terms must be smaller than the truncation error. The magnitude of the numerical damping relative to the leading truncation error term was therefore evaluated for the computed solutions.[14] The root-mean-square value of the damping-to-truncation error ratio was always found to be less than one for all the governing equations. However, the maximum value was an order of magnitude greater in regions of high gradients where the accuracy of the solution was already degraded.

A second evaluation of the numerical error due to damping was performed for the explicit algorithm by comparing the artificial viscosity introduced through the smoothing terms with the real physical viscosity. Comparison[14] of the damping term in the η direction with the normal diffusive terms in the streamwise momentum equation indicated that within the airfoil viscous region, the corresponding artificial viscosity was one order of magnitude smaller than the physical viscosity. However, at the root of the shock, the numerical damping term in the ξ direction became comparable in magnitude to the physical diffusive terms.

V. Conclusions

A critical examination of the numerical solution of high Reynolds number transonic airfoils was performed. Both subcritical and supercritical airfoil flowfields were computed using the two-dimensional Navier-Stokes equations with an algebraic turbulent eddy viscosity model. Two different numerical algorithms were employed, namely, the explicit unsplit MacCormack's scheme and the implicit Beam-Warming algorithm.

The numerical uncertainties associated with different schemes, grid resolution, artificial viscosity, and far-field boundary placement were examined. Results produced by the two numerical schemes were found in very good agreement, with maximum discrepancies that were generally less than the repeatability uncertainties in the experimental measurements. However, further grid resolution, particularly in shock regions still required.

The thin-layer approximation produced essentially the same results as the full Navier-Stokes equations and therefore its use, for this type of flow, is clearly justified.

Comparison of the computed results and the experimental data showed a reasonable prediction of all the essential features of the flow. However, detailed comparison of velocity profiles pointed out deficiencies of the turbulence model in the cove region, downstream of the shock/boundary-layer interaction and in the near wake.

The comparison of computed and experimental results was clouded by uncertainties in the experimental data due to wind tunnel interference effects. Therefore, before a conclusive evaluation of the turbulence model can be conducted, wall interference effects should be properly documented in the experimental study. An alternative approach would consist of numerically solving the three-dimensional wind tunnel flowfield.

Acknowledgments

Computational time for the present calculations was provided in part by the NASA Ames Research Center. The authors also wish to acknowledge Dr. J. Steger, Dr. T. Pulliam, and Mr. T. Barth for several helpful discussions.

References

[1]Mehta, U. and Lomax, H., "Reynolds Averaged Navier-Stokes Computations of Transonic Flows—The State-of-the-Art," *Transonic Aerodynamics*, edited by D. Nixon, Progress in Astronautics and Aeronautics, Vol. 81, AIAA, New York, 1982, pp. 297-375.

[2]Shang, J., "An Assessment of Numerical Solutions of the Compressible Navier-Stokes Equations," AIAA Paper 84-1549, 1984.

[3]Pulliam, T., "Euler and Thin Layer Navier-Stokes Codes: ARC2D, ARC3D," *Notes for Computational Fluid Dynamics*

User's Workshop, The University of Tennessee Space Institute, Knoxville, 1984.

[4]Spaid, W. et al., "An Experimental Study of Transonic Flow About a Supercritical Airfoil," NASA TM-81336, 1983.

[5]Kline, S. et al., *Proceedings of 1980-1981 AFOSR-HTTM-Stanford Conference on Complex Turbulent Flows*, Vol. I, 1982.

[6]Rubesin, M. and Rose, W., "The Turbulent Mean-Flow, Reynolds-Stress and Heat-Flux Equations in Mass Averaged Dependent Variables," NASA TMX-62248, 1973.

[7]Baldwin, B. and Lomax, H., "Thin Layer Approximation and Algebraic Model for Separated Turbulent Flows," AIAA Paper 78-257, 1978.

[8]Visbal, M. and Knight, D., "Generation of Orthogonal and Nearly Orthogonal Coordinates with Grid Control Near Boundaries," *AIAA Journal*, Vol. 20, March 1982, pp. 305-306.

[9]MacCormack, R. W., "The Effect of Viscosity in Hypervelocity Impact Cratering," AIAA Paper 69-354, 1969.

[10]Beam, R. and Warming, R., "An Implicit Factored Scheme for the Compressible Navier-Stokes Equations," *AIAA Journal*, Vol. 16, April 1978, pp. 393-402.

[11]Shang, J. and Hankey, W., "Numerical Solution of the Navier-Stokes Equations for a Three-Dimensional Corner," *AIAA Journal*, Vol. 15, Nov. 1977, pp. 1575-1582.

[12]Pulliam, T. and Steger, J., "Implicit Finite Difference Simulation of Three-Dimensional Compressible Flow," *AIAA Journal*, Vol. 18, Feb. 1980, pp. 159-167.

[13]Visbal, M. and Shang, J., "A Comparative Study Between an Implicit and Explicit Algorithm for Transonic Airfoils," AIAA Paper 85-0480, 1985.

[14]Visbal, M., "Calculation of Viscous Transonic Flows About a Supercritical Airfoil," Air Force Wright Aeronautical Laboratories Tech. Rept., March 1985, in press.

[15]Desideri, J. et al., "On Improving the Iterative Convergence Properties of an Implicit Approximate-Factorization Finite Difference Algorithm," NASA TM-78495, 1978.

[16]Srinivasan, G. et al., "Computation of Simple 3-D Wing-Vortex Interaction in Transonic Flow," AIAA Paper 81-1206, 1981.

[17]Visbal, M. and Knight, D., "The Baldwin-Lomax Turbulence Model for Two-Dimensional Shock-Wave/Boundary-Layer Interactions," *AIAA Journal*, Vol. 22, July 1984, pp. 921-928.

[18]MacCormack, R. and Baldwin, B., "A Numerical Method for Solving the Navier-Stokes Equations with Application to Shock-Boundary Layer Interactions," AIAA Paper 75-1, 1975.

[19]Shang, J. et al., "Performance of a Vectorized Three-Dimensional Navier-Stokes Code on a CRAY-1 Computer," *AIAA Journal*, Vol. 18, Sept. 1980, pp. 1073-1079.

[20]Steger, J., "Implicit Finite-Difference Simulation of Flow About Arbitrary Two-Dimensional Geometries," *AIAA Journal*, Vol. 16, July 1978, pp. 679-686.

[21]Chyu, W. and Kuwahara, K., "Computations of Transonic Flow Over an Oscillating Airfoil with Shock-Induced Separation," AIAA Paper 82-0350, 1982.

[22]Degani, D. and Steger, J., "Comparison Between Navier-Stokes and Thin-Layer Computations for Separated Supersonic Flow," *AIAA Journal*, Vol. 21, Nov. 1983, pp. 1604-1606.